

# Digital holographic microscopy for nanometric quality control of micro-optical components

Jonas Kühn<sup>\*a</sup>, Florian Charrière<sup>a</sup>, Tristan Colomb<sup>a,c</sup>, Etienne Cuche<sup>b</sup>, Yves Emery<sup>b</sup>  
and Christian Depeursinge<sup>a</sup>

<sup>a</sup>Ecole Polytechnique Fédérale de Lausanne (EPFL), Institute of Imaging and Applied Optics,  
CH-1015 Lausanne, Switzerland;

<sup>b</sup>Lyncée Tec SA, PSE-A, CH-1015 Lausanne, Switzerland, [www.lynceotec.com](http://www.lynceotec.com);

<sup>c</sup>Centre de Neurosciences Psychiatriques, Département de psychiatrie DP-CHUV, Site de Cery,  
CH-1008 Prilly- Lausanne, Switzerland

## ABSTRACT

In this paper, Digital Holographic Microscopy (DHM) is presented as a powerful tool for quality control of micro-optical components. It will be shown that not only the single-shot full field-of-view nanometer axial resolution makes DHM an ideal solution for such samples, but the DHM numerical wavefront correction formalism is perfectly adapted to provide advanced features like aberration coefficients, radius of curvature or optical surfaces roughness measurements. Both transmission and reflection configurations can be used depending of the micro-components under investigation. A transparent high aspect-ratio micro-components investigation procedure is also exposed in order to unambiguous phase unwrapping. Each feature is illustrated with typical examples, ranging from a wide variety of micro-lenses (aspherical, cylindrical, squared) to cornercube micro-structures or diffractive elements.

Keywords: Metrology, microscopy, digital holography, micro-optics, micro-lenses, aberrations

## 1. INTRODUCTION

The technique currently known as “Digital Holography” (DH), even if discovered much earlier<sup>1</sup> has really become a reality only in the early 90’ when the arrival of the first Charge Coupled Device (CCD) digital cameras and the microscale pixel sizes made it possible to record an hologram on an electronic device and store it on a computer for further software treatment<sup>2, 3</sup>. Said simply, instead of illuminating an object with a coherent beam and recording the interference with a reference beam from the same source on a photosensitive plate like in classical holography<sup>4</sup>, in DH the hologram is captured by a CCD camera and thereafter the reconstruction process is all-digital. The complex wavefront in the hologram plane can be easily retrieved and numerically propagated in a discrete version of the Fresnel approximation to an observation plane, typically the object plane, and both the amplitude and especially the phase can be computed in real time<sup>5, 6</sup>. The capability to have a quantitative access to the phase information provides an axial resolution in the nanometer range, while the lateral resolution remains diffraction- or pixel-limited. Later on, Cuche *et al.* demonstrate that a Microscope Objective (MO) could be used in a DH setup to magnify the object image<sup>7</sup>, thus overcoming the pixel size Nyquist sampling limitation and providing a true diffraction-limited lateral resolution, down to a few hundreds of nanometer depending of the numerical aperture (NA) of the MO.

This Digital Holographic Microscopy (DHM) technique simultaneously exhibits real-time video-frequency capability, robustness in regards to the environmental conditions (micro-seconds CCD shutter time), digital focusing properties, strictly non-invasive operation and a full-frame nanometer vertical resolution. It has already been successfully applied in various fields, let us just mention biological cells monitoring<sup>8</sup>, MEMS/MOEMS dynamic observation with or without stroboscopic operation<sup>9, 10</sup>, state-of-polarization imaging<sup>11</sup> or multi-wavelength tomography without mechanical scanning<sup>12, 13</sup>. Moreover, DHM opens new opportunities regarding the possibility to digitally compensate for aberrations<sup>14</sup> and recently Colomb *et al.* even introduced a whole new formalism of “numerical optics”, called Numerical Parametric Lenses (NPL)<sup>15</sup>.

\*jonas.kuehn@a3.epfl.ch, phone +41216933742, fax +41216933701; <http://apl.epfl.ch/page12232.html>

These last approaches are particularly relevant for the inspection of micro-optics components because, set aside the delivery of a phase-contrast image of the specimen free of setup aberrations, they easily make possible to extract the Zernike polynomial aberration coefficients of the sample with a wavefront precision below  $\lambda/100$  or to compute the radius of curvature (ROC). The information is in fact available in real-time, which is useful for example to implement a quality control of a micro-lenses array production directly on the conveyor belt. In top of that, the methodology of Colomb *et al.* also enables to numerically remove a form-factor, in other words “flattening” the sample, for example in order to compensate for the curvature of an aspheric lens in order to measure the roughness of its optical surface.

The paper reviews some examples of such DHM measurements for various micro-optical components, namely aspherical, cylindrical and square lenses. Characteristics like lens height, ROC, aberrations coefficients and surface roughness are measured. Other micro-structures like diffractive Fresnel lenses or transparent micro-cornercubes are also investigated. These last ones require a specific procedure to resolve the phase jumps present with high aspect-ratio micro-components, and a solution with the use of two successive immersion liquids to retrieve the topography without knowledge of the sample refractive index is briefly presented.

## 2. METHODOLOGY

### 2.1 Principle of Digital Holographic Microscopy

Depending on the sample to be investigated, two off-axis setup configurations can be implemented for DHM: a reflection arrangement for reflective or semi-reflective objects (e.g. metallic surfaces), and a transmission one for transparent or quasi-transparent samples (e.g. living cells). Both experimental arrangement for DHM are depicted in Fig. 1. Generally the interferometer setups are based on a Mach-Zehnder configuration, but a Michelson type DHM may be used for reflection measurement if compactness and cost are an issue.

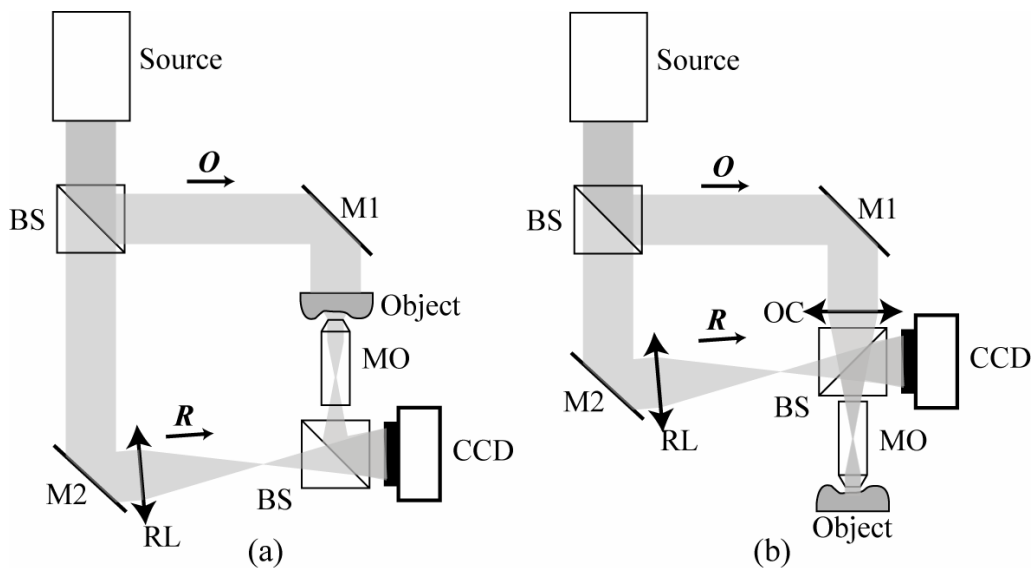


Figure 1. DHM Setup configurations. (a) Transmission DHM; (b) Reflection DHM; O, object wave; R, reference wave; BS, beam-splitter; M1, M2 mirrors; OC, objective condenser lens; RL, reference lens, which matches the curvature induced on the object wave by the microscope objective (MO)

Essentially, the interference between the object beam and the reference arm is recorded on the CCD camera, forming the digital hologram. As can be seen above on Fig. 1, no moving parts like piezo-actuators or scanning-mirrors are presents in the optical design resulting in simplified operations, improved accuracy, high robustness and - as will be demonstrated - real-time imaging with a single acquisition without the use of multiple phase-shifting exposures.

The resulting hologram intensity  $I_H$  recorded on the CCD camera can be expressed as follows:

$$I_H(x, y) = |\mathbf{R}|^2 + |\mathbf{O}|^2 + \mathbf{R}\mathbf{O}^* + \mathbf{R}^*\mathbf{O} \quad (1)$$

As the off-axis configuration is used here, it's straightforward to Fourier-filter either one of the last two inference terms (the real or the virtual image) in the 2D-Fourier domain, while the zero-order reverts no particular interest and should be discarded. The selected complex wavefront is afterward numerically propagated in the Fresnel approximation by a software program running on a computer. The discrete expression of the wavefront in the convolution formulation is the one of Eq. 2:

$$\Psi_{CF}(m, n) = \Gamma^I(m, n) \cdot \frac{\exp(i2\pi d / \lambda)}{i\lambda d} \cdot FFT^{-1} \left\{ FFT[\Gamma^H(k, l) I_H^F(k, l)] \cdot \exp \left[ -i\pi\lambda d \left( \frac{k}{N\Delta x} \right)^2 - i\pi\lambda d \left( \frac{l}{N\Delta y} \right)^2 \right] \right\} \quad (2)$$

Where  $\Psi_{CF}$  is the reconstructed wavefront in the convolution formulation,  $\Gamma^I$  and  $\Gamma^H$  are digital phase masks (DPM) in the image and hologram planes used to compensate for aberrations (see section §2.2),  $d$  is the propagation distance,  $FFT$  is the Fast Fourier Transform operator,  $I_H^F$  is the Fourier-filtered hologram of Eq. 1,  $k$ ,  $l$ ,  $m$  and  $n$  are integers ( $-N/2 \leq k, l, m, n < N/2$ ) representing coordinates in the hologram plane, respectively the reconstruction plane,  $NxN$  is the number of pixels of the CCD camera and  $\Delta x$  and  $\Delta y$  are the pixel size of CCD. In other words, for the simple free-space configuration with plane waves the illumination of the developed hologram plate, like in classical holography, is simulated by approximating the hologram as a transmittance device and multiplying it by a “digital reference wave”  $R_D$  as DPM  $\Gamma_H$  and emulating the re-illumination of the hologram. Such a case can be expressed as follows:

$$\Gamma_H(k, l) = R_D(k, l) = \exp[i(k_x k \Delta x + k_y l \Delta y)] \quad (3)$$

with  $k_x$  and  $k_y$  the tilt parameters.

By having quantitative values for the complex wavefront reconstructed in the object plane, it's simple to extract its amplitude and phase components at each pixel. This last information leads to nanometric-range axial resolution, providing that the reference wave tilt and setup aberrations are digitally compensated (see next section §2.2). Typical experimental values are around  $2^\circ$  phase standard deviation over the whole field-of-view (FOV), corresponding to about 2nm at 633nm wavelength for direct reflection measurements in air.

## 2.2 Digital phase mask adjustment procedure and aberrations correction

The methodology briefly described here has already been discussed in depth in previous publications<sup>14, 15</sup>, it essentially consists in polynomial fitting procedure based on an a-priori knowledge of the specimen. A lot of samples are indeed composed of known-flat or reference areas easily recognizable in the amplitude image, so the user has only to draw 1D-segments<sup>14</sup> or 2D-shapes<sup>15</sup> on these image regions, then an automatic procedure fit the desired polynomial order on the selected points in the mean square sense. Let's take the example of a configuration with only tilt and 2<sup>nd</sup> order aberration (usually induced by the MO): in this case the user has only to draw one horizontal and one vertical segment, giving two 1-dimensional arrays of values that can be fitted to a polynomial model of order two, leading to the following expression:

$$\begin{aligned} Y_h &= a_0 + a_1 x + a_2 x^2 \\ Y_v &= b_0 + b_1 y + b_2 y^2 \end{aligned} \quad (4)$$

where  $Y_h$  and  $Y_v$  are the two sets of data acquired along the horizontal and the vertical profiles,  $x$  and  $y$  are the pixel position and  $a_i$  and  $b_i$  are the fitted coefficients of the 2<sup>nd</sup> order polynomial model .

From these fitted coefficients, it's now possible to express the polynomial phase mask (DPM) as follows, in either the hologram ( $I_H$ ) or image plane ( $I_I$ ):

$$\Gamma_{H,I}(m,n) = \exp[-i(a_1m + b_1n + a_2m^2 + b_2n^2)] \quad (5)$$

The DPM  $\Gamma$  of Eq. 5 is then inserted in the reconstruction procedure of Eq. 2, correcting the wavefront for a first iteration, then a new fitting iteration is executed, the DPM is updated, and so on until all tilt and defocus aberrations are compensated, thus yielding an adjusted reconstructed object wave. This approach is the very reason why digital reconstruction of holograms without phase-shifting sequential acquisitions can be achieved, paving the way to real-time DHM. An example of the method is illustrated on Fig. 2 for a USAF test target (chromium deposit on glass substrate) measured in reflection:

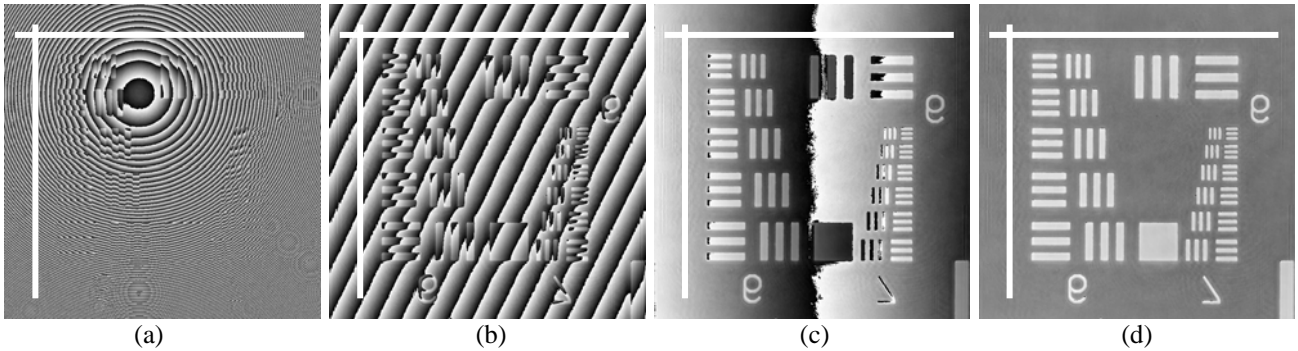


Figure 2. DPM polynomial adjustment over a USAF test target, with two segments drawn by the user.

- (a) Raw phase-contrast image with tilt and defocus aberration;
- (b) Phase image after one iteration: only the tilt aberration remains;
- (c) Phase image after two iterations: only a small horizontal tilt aberration remains, the vertical one being already corrected ;
- (d) Adjusted phase reconstruction after three iterations.

As demonstrated in Fig. 2, only a few iterations are necessary to entirely compensate for aberrations. Increasing the polynomial order allows to compensate for higher aberrations order.. Let us also point out that for objects with no reference areas to be selected on, or for routine use, a pre-calibration of a setup on a reference mirror (or without sample for transmission DHM) corrects all high-order aberrations on a persistent manner, so each experiment doesn't necessitate to perform the procedure each time except for a simple 1<sup>st</sup> order tilt compensation, often largely due to the object holder itself.

More interestingly a two-dimensional approach can also be implemented<sup>14</sup> which enables to perform the fitting procedure on entire sample 2D-areas with a matrix mean square error reduction formalism, in particular opening the way to a Zernike polynomial model compatibility. The adjustment of the Zernike coefficients to compensate for aberrations are essential for the applications presented here, because these coefficients give a quantitative evaluation of optical quality of investigated lenses. One should note that the definition of the fitting areas can be defined by the operator, but automatic shape recognition feature can be easily implemented to make the method ideal for micro-optics inspection. Examples are proposed in the next section.

### 3. MEASUREMENTS

#### 3.1 Micro-lenses inspection

Refractive micro-lenses are used in a lot of applications nowadays, and there is a strong need to assess the optical quality and to quantify the phase function of each device in a production environment. The stylus probe approaches for example cannot evaluate the optical transfer function, but only the surface shape. Comparative methods, with a reference sample, or other interferometric techniques offer solutions but they are often either unable to deliver quantitative results for phase function or suffer from a low speed scanning process or a high-sensitivity to environmental conditions, critical for production inspection. As shown on Fig. 3, DHM provides a non-contact quantitative phase measurement of spherical transparent micro-lenses array, with a single acquisition:

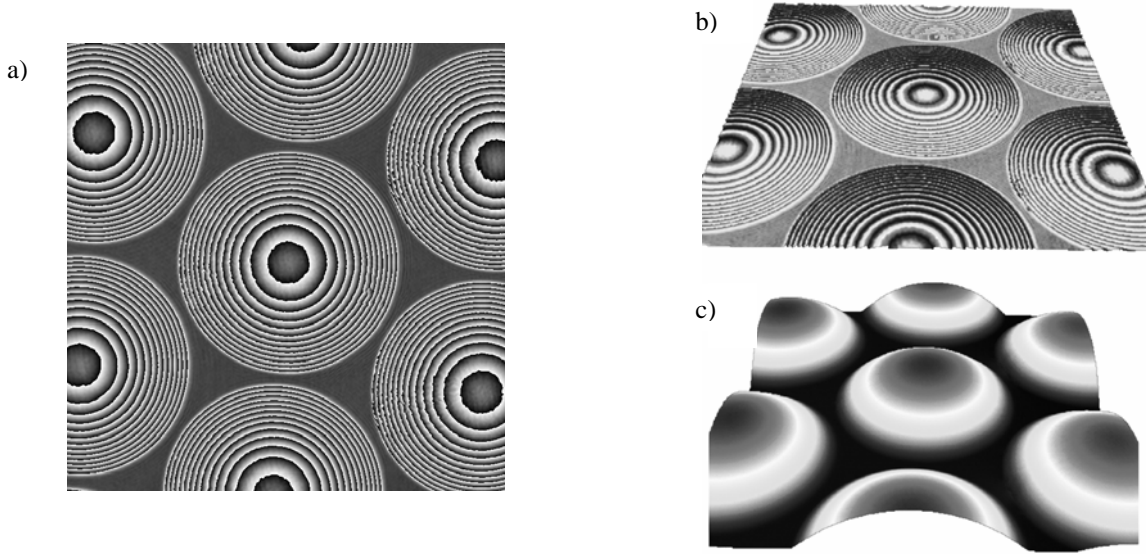


Figure 3. (a) Raw phase-contrast image of a micro-lenses array obtained by a 10x DHM in transmission mode,  $\lambda = 664$  nm, FOV  $\sim 0.5 \times 0.5$  mm; (b) 3D perspective of (a); (c) Unwrapped 3D perspective of (a)

As can be seen in Fig. 3, it is necessary to use an unwrapping algorithm to retrieve the true optical path length map of the specimen, because the phase is only defined *modulo*  $2\pi$ . It should also be noted that the unwrapping algorithm works only if the phase jumps are laterally resolved, so the smaller the radius of curvature (ROC), the higher the MO magnification should be (or an immersion medium can be used, see section §3.3). In top of that, an a-priori knowledge of the refractive index is mandatory to compute the true topography of the object for transmission, otherwise a decoupling procedure like the one presented in section §3.3 is needed. If the sample refractive index is known and homogeneous one can easily obtain the height according to Eq. 6:

$$h = \frac{\lambda}{2\pi} \frac{\phi}{(n_S - n_L)} \quad (6)$$

where  $h$  is the height of the object (or sum of both sample sides topography),  $\lambda$  the wavelength,  $\phi$  the measured phase in radian,  $n_S$  the specimen refractive index and  $n_L$  the medium refractive index (usually air, so  $n_L = 1$ ).

Valuable information can be extracted from the topographic map, noticeably the micro-lenses height, diameter and ROC, as can be seen in Fig. 4 with a refractive spherical micro-lens of theoretical ROC of 348 $\mu\text{m}$ :

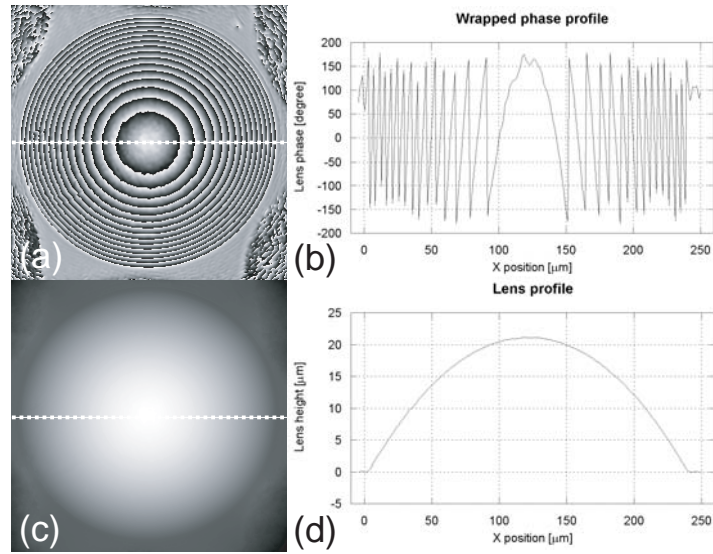


Figure 4. Micro-lens measurements with a 20x 0.5NA DHM in transmission,  $\lambda = 664 \text{ nm}$ , FOC  $\sim 250 \times 250 \mu\text{m}$ ;  
 (a) Wrapped phase image; (b) Profile line extracted along the white segment in (a), the phase jumps are clearly visible;  
 (c) Unwrapped phase image; (d) Same of profile as (b) taken from (c), this time the profile is unwrapped and free of phase jumps

The refractive lens diameter measured in Fig. 4 is 240  $\mu\text{m}$  and the height is 21.15  $\mu\text{m}$ . From these values, the ROC is deduced according to Eq. 6:

$$ROC = \frac{h}{2} + \frac{D^2}{8h} \quad (6)$$

where  $h$  is the measured height, and  $D$  the diameter.

From Eq. 6 the ROC measured for this micro-lens is 351  $\mu\text{m}$ , which matches well the theoretical value of 348  $\mu\text{m}$ .

To further validate the quantitative results obtained by DHM, we compare the results of our method with a stylus probe Alpha step apparatus (Alpha step 200 from Tencor Instrument) for reflective Si micro-lenses, as presented on Fig. 5:

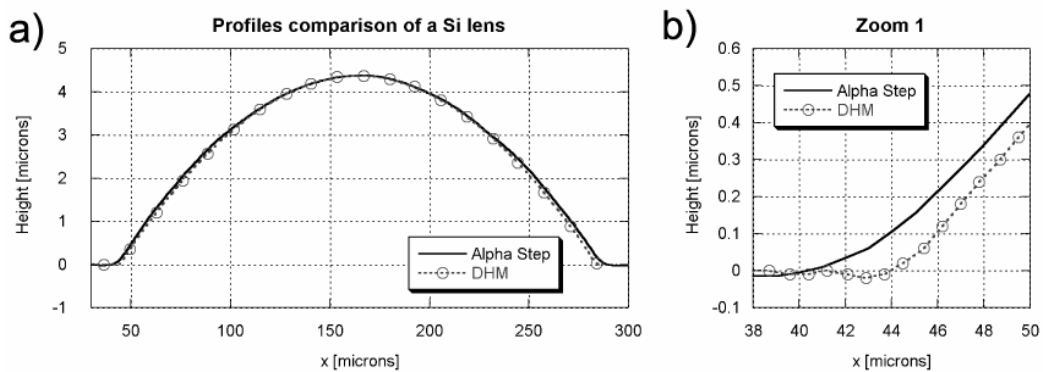


Figure 5. (a) Profile comparison between a DHM and an Alphas Step measurement on a reflective Si lens; (b) Zoom on the lens border

The profiles of Fig. 5 are in good concordance, except a small deviation of the initial slope at the border of the lens. This can be mainly explained by the nature of the probe technique, which can be described as a convolution between the tip of the stylus and the specimen shape, especially visible for regions with an abrupt variation of height.

Even if the results presented here are extremely useful, it's not straightforward to extract the phase transfer function and the Zernike coefficients from these values. However the very same DPM adjustment procedure presented in section §2.2 can be directly applied to “flatten” the micro-lens under investigation using a two-dimensional Zernike polynomial model<sup>15</sup>. As demonstrated below in Fig. 6, the progressive increase in Zernike coefficients fit order not only fully compensate for the micro-lens shape but the fitted coefficients represent the aberration or phase function of the optics under investigation:

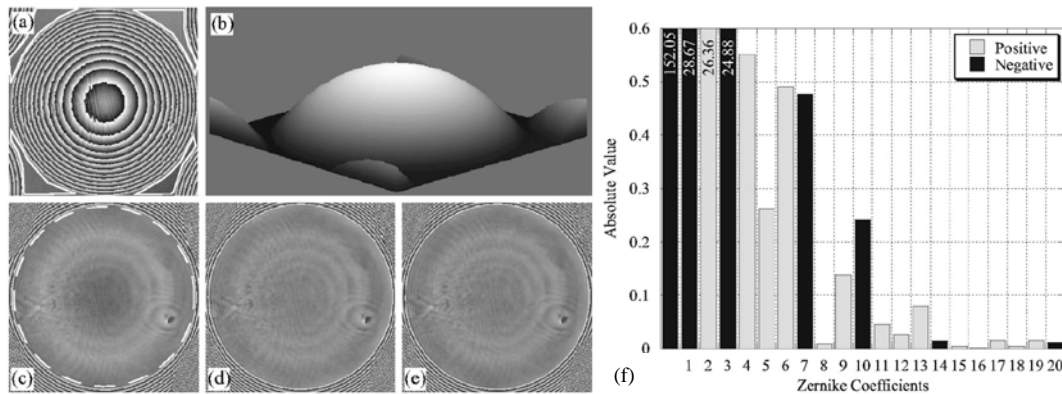


Figure 6. (a) Raw phase image of the same micro-lens as Fig. 3; (b) 3D Perspective of 2D-unwrapped (a); (c) Parameters-adjusted phase image by taking the lens itself as reference surface (white dashed circle) and use of 10 Zernike polynomials; (d) Same as (c) but with 11 parameters (spherical aberration added); (e) Same as (c) but with 21 parameters; (f) Absolute values and weights of each Zernike coefficients for (e)

Different information can be extracted from the results depicted in Fig.6, especially the Zernike coefficients are giving the phase aberrations of the micro-lens (transmission transfer function) and their respective weights are a good representation of which aberration is dominating. Indeed, one can observe that there is a major improvement in phase correction between Fig. 6d over Fig. 6c because the 11<sup>th</sup> Zernike polynomial term - the spherical aberration - plays a major role in the global phase function of micro-lens, which is expected from a spherical lens. On the other hand the increase in polynomial order from Fig. 6d to Fig. 6e doesn't really change anything in term of correction, so this micro-lens could be well described with only the 11<sup>th</sup> order Zernike model up to the spherical term. In addition to obtaining the complete Zernike model description of the micro-optics under investigation, this kind of “flattened” image can also give information about the surface roughness of the object as shown in Fig. 7:

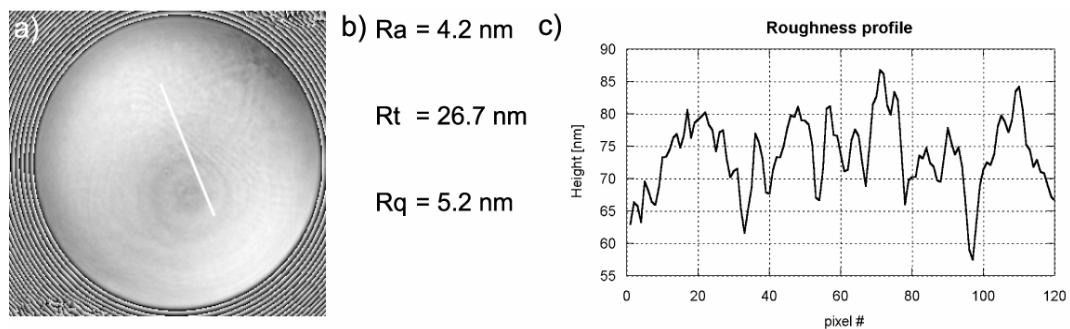


Figure 7. (a) Curvature-corrected phase image of a Si-lens measured in reflection; (b) Roughness parameters extracted from the white line profile in (a); (c) Topographic profile taken along the same white line profile in (a)

As demonstrated above in Fig. 7, once the shape parameters of the micro-lens are removed by the fitting procedure it's easily possible to measure surface roughness parameters on the resulting phase image. Let us remind that single-surface characterization is strictly valid only for reflective measurements, as transmission results represent an integrated roughness between the upper and lower side of the micro-structure, thus still relevant in a lot of situations.

Overall DHM is a powerful tool for micro-lenses investigation by being able to provide simultaneously quantitative ROCs, heights, Zernike coefficients and roughness parameters for all samples in the field-of-view. The real-time capability of DHM makes possible to obtain these data live in a production environment, while keeping the robustness and nanometer-range vertical resolution advantages of the technique.

### 3.2 Other micro-optics measurements

In addition to spherical or aspherical micro-lenses investigation, a wide variety of other micro-optics components can be successfully characterized by DHM. For example, Fig. 8 presents results obtained with a cylindrical lens in transmission configuration:

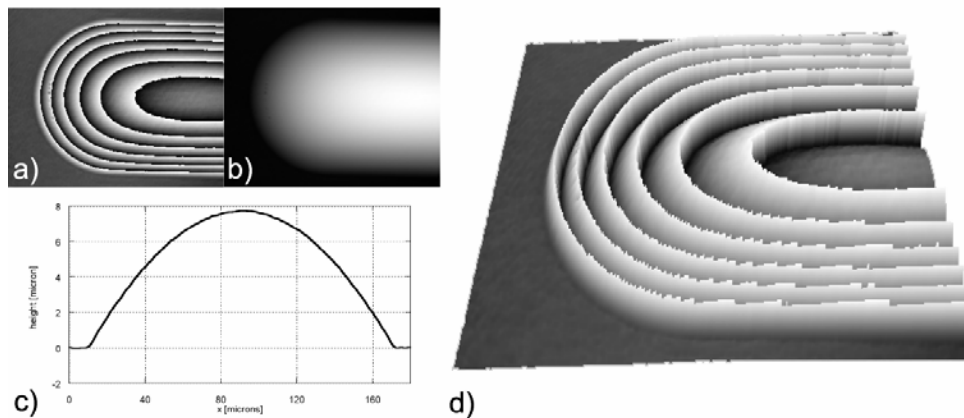


Figure 8. (a) Raw phase-contrast image of a transparent quartz cylindrical micro-lens obtained with a reflection 20x 0.5NA DHM (lens diameter 160  $\mu\text{m}$ , maximal measured height 7.73  $\mu\text{m}$ , measured ROC 417.8  $\mu\text{m}$ ); (b) 2D-unwrapped image of (a); (c) Plot of a profile line taken transversally across the sample in (b); (d) 3D perspective of (a)

Figure 8 clearly illustrates the versatility of DHM regarding the variety of micro-optics shapes which can be imaged and quantitatively characterized. Let us also point out that this measure is realized in a reflection arrangement even if the cylindrical micro-lens was transparent, so even a small back-reflected signal might be enough for DHM. This strongly depends on the lens curvature, the working distance (WD) and the numerical aperture (NA) of the MO. For the sake of completeness Fig. 9 illustrates the same type of measurements for square micro-lenses:

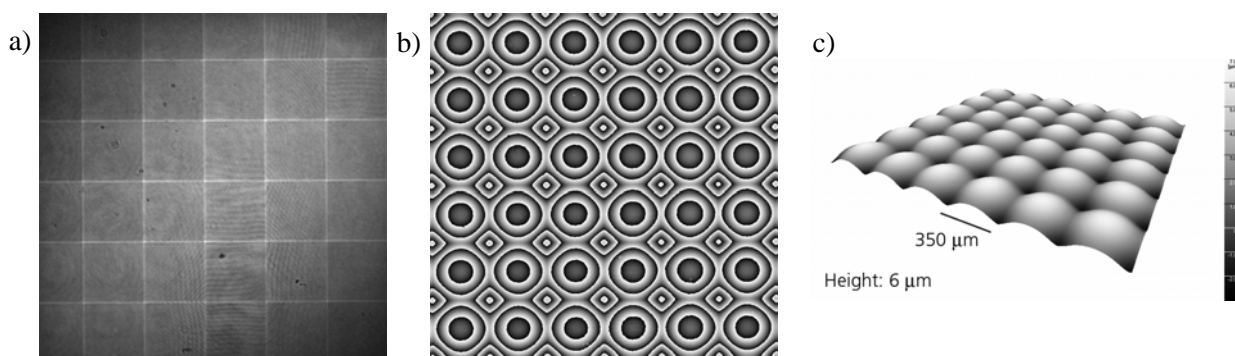


Figure 9. (a) Amplitude image of square micro-lenses array with a 2.5x transmission DHM; (b) Phase image of the same sample; (c) Unwrapped 3D Perspective of (b)

Another type of micro-optical components are Fresnel lenses, and Fig. 10 depicts an experiment with 250  $\mu\text{m}$  diameter Fresnel lenses observed with 10x DHM in transmission, compared with a measurement with the same Alpha-step device as in Fig. 5:

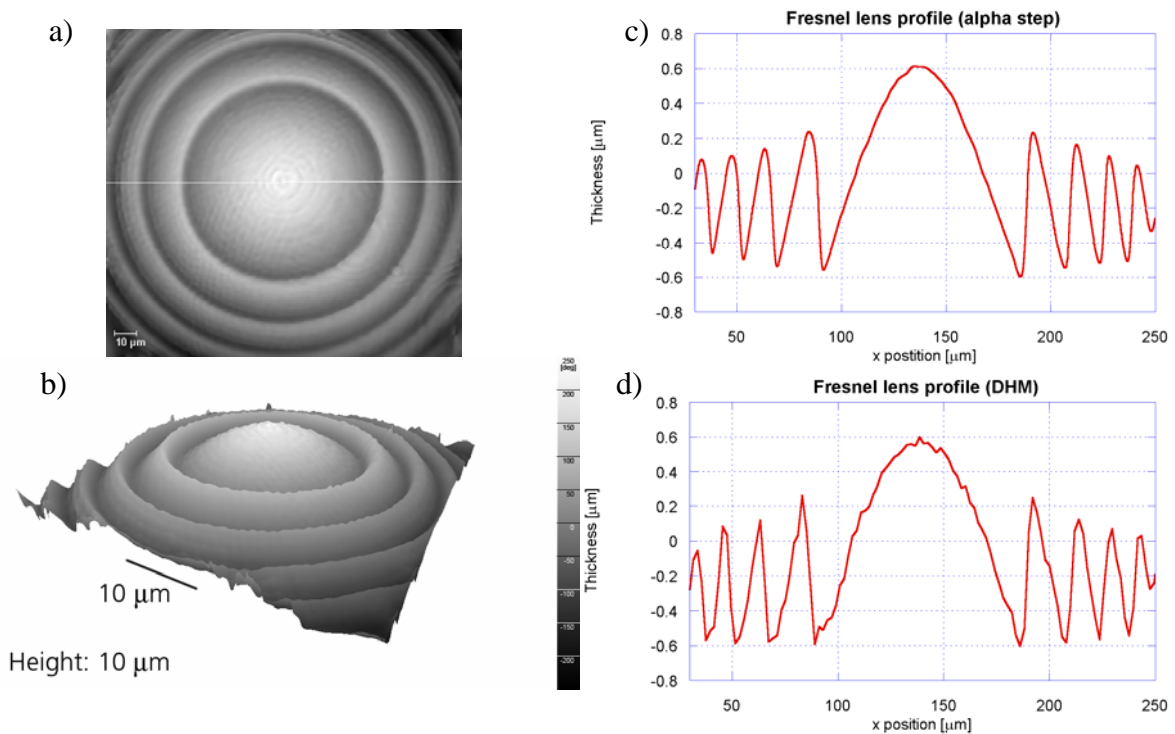


Figure 10. (a) 20x DHM phase image of 250 $\mu\text{m}$  Fresnel lenses; (b) 3D perspective of (a); (c) Measured profile of the structure with a stylus probe Alpha-step 200; (d) Measured DHM profile taken across the white line profile in (a)

The results of Fig. 10 require some comments. First the periodic annular phase steps of Fig. 10a are not phase jumps but the very diffractive structure of the Fresnel lens. Secondly the DHM profile of Fig. 10d is noisier than the stylus probe one of Fig. 10c, due to the diffractive nature of the specimen. A better approximation of diffraction than the Fresnel formulation would be required to enhance the quality of the measure. And finally, the Alpha-step profile of Fig. 10c is smoothed compared to the DHM results because the tip diameter is about 12 $\mu\text{m}$  and thus cannot reach the bottom and upper parts of each diffractive digs and tips. All in all, DHM measurements are more precise regarding the total height of the structure for this reason, plus a whole array of micro-components can be investigated in one single acquisition compared to the scanning nature of the probe method.

### 3.3 High aspect-ratio microstructures measurements and sample refractive index determination

In all experiments presented before the phase jumps were resolved because the samples slopes or ROCs were not too high, and the MO magnification and NA were large enough to resolve them so 1D- or 2D-unwrapping procedures could be used. However for high aspect-ratio objects this condition is not always fulfilled. For transparent micro-structures of this kind, we propose a method which makes use of an immersion liquid in order to artificially reduce the optical path difference (OPD) between adjacent points of a strong slope, thus reducing the phase jumps occurrence. This situation is illustrated on Fig. 11:

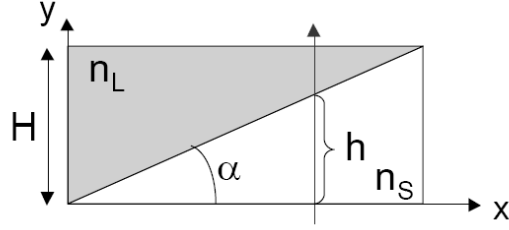


Figure 11. Measurement of the slope of an object in an immersion liquid.  $H$ , total height;  $n_s$  refractive index of the sample;  $n_L$  refractive index of the immersion liquid;  $\alpha$  angle of the slope to measure

From Fig. 11 we can easily write the phase  $\phi$  of each points along the  $x$  axis:

$$\phi(x) = \frac{2\pi}{\lambda} OPL(x) = \frac{2\pi}{\lambda} \{n_s h(x) + n_L [H - h(x)]\} = \frac{2\pi}{\lambda} [(n_s - n_L)h(x) + n_L H] \quad (7)$$

with  $OPL$  being the optical path length.

And the apparent slope is now:

$$p = \frac{d\phi(x)}{dx} = \frac{2\pi}{\lambda} (n_s - n_L) \frac{dh(x)}{dx} \quad (8)$$

Clearly in Eq. 8 the apparent slope is now reduced because the factor  $(n_s - n_L)$  is usually inferior to unity, the singular case being when the specimen index is matched by the immersion medium so the structure is “invisible” in phase. This is illustrated thereafter in Fig. 12:

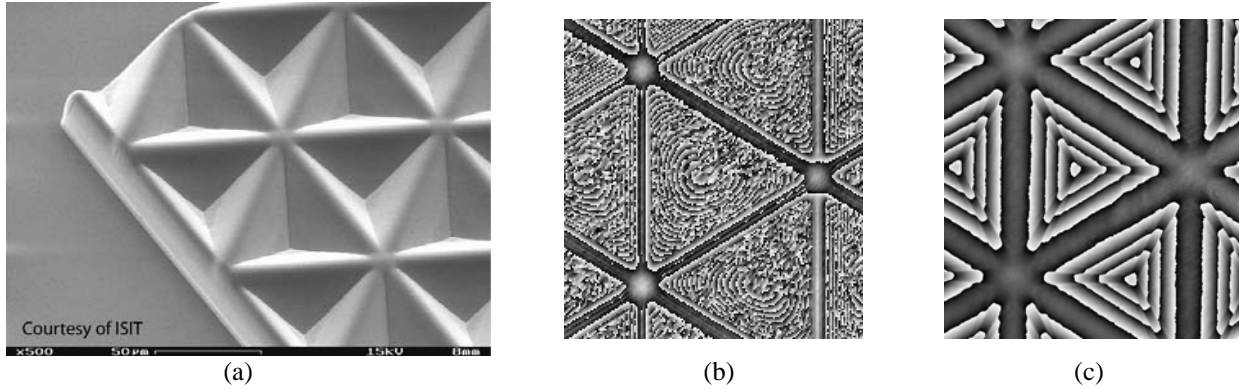


Figure 12. (a) Metal shim of 50 microns tetrahedral transparent micro-cornercubes array observed with SEM; (b) Phase image in air with a 60x 0.65NA DHM in transmission, FOV ~ 0.1 x 0.1 mm; (c) Same as (b) but in an calibrated immersion liquid of refractive index  $n_L = 1.45$

This kind of aspect-ratio reduction in phase shown on Fig. 12 can be used on all transparent sort of micro-components, providing there are no direct step or jump of OPL. Then it's straightforward to obtain the topography by integrating Eq. 8 to obtain Eq. 6 if the refractive index of the object is known. If not, one can use a two-steps procedure by performing two successive DHM phase measurements in two different immersion liquids of indexes  $n_{L1}$  and  $n_{L2}$ , so we obtain two slopes  $p_1$  and  $p_2$  and the sample refractive index is then obtained by the following expression:

$$n_s = \frac{p_1 n_{L2} - p_2 n_{L1}}{p_1 - p_2} \quad (9)$$

Experimentally to use Eq. 9 one has only to take the two profiles for examples across one face of the tetrahedron of Fig. 12c, than proceed as illustrated in Fig. 13:

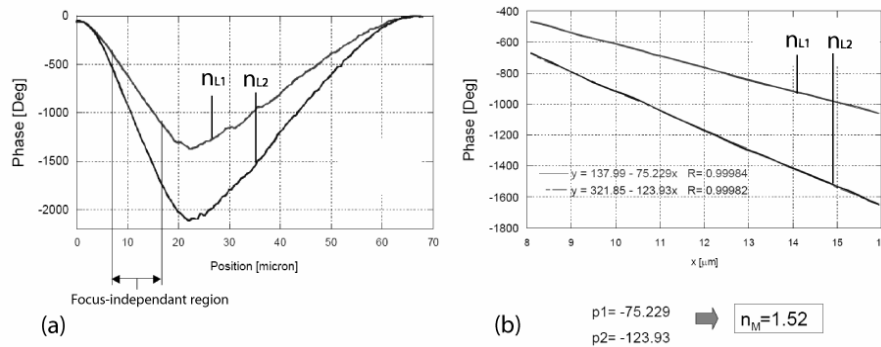


Figure 13. (a) Phase profiles across one face of the tetrahedron of Fig. 12c for two different immersion mediums; (b) 1<sup>st</sup> order polynomial fit on the focus-independent regions of the profiles of (a), giving the two slopes from which the sample refractive index  $n_s = n_m$  can be obtained according to Eq. 9.

The focus-independent region from which the slopes are extracted in Fig. 13 is the one within the depth of field of the MO. It's an important parameter for high aspect-ratio micro-structures over several microns in height and this serious limitation should not be neglected when choosing the magnification to image the object. Generally speaking, the lower the magnification of the MO the higher the depth of field, but the lower the lateral resolution so the harder it is to resolve the phase jumps of high aspect-ratio specimens unless the immersion liquids are near-matched to the sample refractive index.

We have shown here that it's possible to image high aspect-ratio micro-components like transparent micro-cornercubes arrays with DHM by using one or more immersion mediums, and thus enabling quantitative study of these components like e.g. in Fig. 14 where each face angles of the tetrahedron are precisely measured:

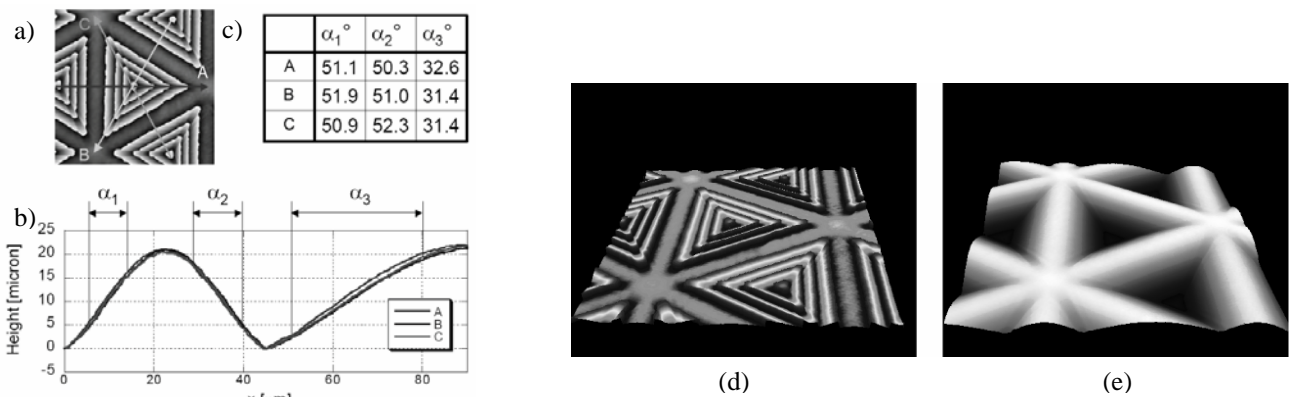


Figure 14. (a) Same as Fig. 12c with extraction of three profiles on the phase image; (b) Profiles A, B et C according to (a) with the focus-independent regions where the slopes are computed; (c) Calculated angles for the faces and edges of (a) as depicted in (b); (d) 3D perspective of (a); (e) Unwrapped 3D perspective of (a) leading to the true topography of the micro-component

#### 4. CONCLUSIONS

We herein present the DHM technique applied to quantitative micro-optical components characterization, and illustrate this for a wide variety of samples: spherical or aspherical lenses, cylindrical lenses, square lenses, Fresnel lenses and high aspect-ratio micro-cornercubes. Not only DHM achieves real-time nanometer-range axial resolution compatible with a production environment, but we have shown that it delivers a comprehensive range of useful quantitative information about the samples investigated: topographic maps, 1D-profiles, radius-of-curvature, Zernike transfer function coefficients, surface roughness parameters, refractive index and precise edge angles. Some measurements are

compared to results obtained with stylus-probe techniques or available information from manufacturers, and they appeared on good agreement. The illustrated features and other which are not exposed here, like numerical focusing by varying the propagation distance, make DHM a very competitive technology for micro-optical components inspection. Indeed, the capability to access all the range of measurements on micro-optics exposed in this paper with a single technique is to the extend of our knowledge a singularity not matched by other metrological technology until now.

## 5. ACKNOWLEDGEMENTS

The development of the technology has been supported by the Swiss government through the Swiss National Science Foundation (SNSF) grant #205320-103885/1 and CTI grants #6103.3 and #6606.2. Systems are commercialized by Lyncée Tec SA (<http://www.lynceetec.com/>).

## REFERENCES

1. J. W. Goodman, and R. W. Lawrence, "Digital image formation from electronically detected holograms," *Applied Physics Letters* **11**, 77-79 (1967).
2. O. Coquoz, C. Depeursinge, R. Conde, and F. Taleblou, "Numerical reconstruction of images from endoscopic holograms," in *14th Annual International Conference of the IEEE-EMBS*, (IEEE, Paris, 1992), pp. 338-339.
3. U. Schnars, and W. Jüptner, "Direct Recording of Holograms by a Ccd Target and Numerical Reconstruction," *Applied Optics* **33**, 179-181 (1994).
4. D. Gabor, "A New Microscopic Principle," *Nature* **161**, 777-778 (1948).
5. U. Schnars, "Direct phase determination in hologram interferometry with use of digitally recorded holograms," *J. Opt. Soc. Am. A* **11**, 2011-2015 (1994).
6. E. CuChe, F. Bevilacqua, and C. Depeursinge, "Digital holography for quantitative phase-contrast imaging," *Optics Letters* **24**, 291-293 (1999).
7. E. CuChe, P. Marquet, and C. Depeursinge, "Simultaneous amplitude-contrast and quantitative phase-contrast microscopy by numerical reconstruction of Fresnel off-axis holograms," *Applied Optics* **38**, 6994-7001 (1999).
8. P. Marquet, B. Rappaz, P. J. Magistretti, E. CuChe, Y. Emery, T. Colomb, and C. Depeursinge, "Digital holographic microscopy: a noninvasive contrast imaging technique allowing quantitative visualization of living cells with subwavelength axial accuracy," *Optics Letters* **30**, 468-470 (2005).
9. G. Coppola, M. Iodice, A. Finizio, S. D. Nicola, G. Pierattini, P. Ferraro, C. Magro, and G. E. Spoto, "Digital holography microscope as tool for microelectromechanical systems characterization and design," *Journal of Microlithography, Microfabrication, and Microsystems* **4**, 013012 (2005).
10. Y. Emery, E. CuChe, F. Marquet, N. Aspert, P. Marquet, J. Kühn, M. Botkine, T. Colomb, F. Montfort, F. Charrière, C. Depeursinge, P. Debergh, and R. Conde, "Digital Holographic Microscopy (DHM) for metrology and dynamic characterization of MEMS and MOEMS - art. no. 61860N," in *Mems, Moems, and Micromachining II*, H. Urey, and A. ElFataty, eds. (Spie-Int Society Optical Engineering, Bellingham, 2006), pp. N1860-N1860.
11. T. Colomb, P. Dahlgren, D. Beghuin, E. CuChe, P. Marquet, and C. Depeursinge, "Polarization imaging by use of digital holography," *Applied Optics* **41**, 27-37 (2002).
12. M. K. Kim, "Tomographic three-dimensional imaging of a biological specimen using wavelength-scanning digital interference holography," *Optics Express* **7**, 305-310 (2000).
13. F. Montfort, T. Colomb, F. Charrière, J. Kühn, P. Marquet, E. CuChe, S. Herminjard, and C. Depeursinge, "Submicrometer optical tomography by multiple-wavelength digital holographic microscopy," *Applied Optics* **45**, 8209-8217 (2006).
14. T. Colomb, E. CuChe, F. Charrière, J. Kühn, N. Aspert, F. Montfort, P. Marquet, and C. Depeursinge, "Automatic procedure for aberration compensation in digital holographic microscopy and applications to specimen shape compensation," *Applied Optics* **45**, 851-863 (2006).
15. T. Colomb, F. Montfort, J. Kühn, N. Aspert, E. CuChe, A. Marian, F. Charrière, S. Bourquin, P. Marquet, and C. Depeursinge, "Numerical parametric lens for shifting, magnification and complete aberration compensation in digital holographic microscopy," *Journal of the Optical Society of America A-Optics Image Science and Vision* **23**, 3177-3190 (2006).